



HAL
open science

3D-Modeling of thermal degradation of spruce wood under inert atmosphere

Hassan Flity, Mariam Abdo, Lucas Terrei, Zoubir Acem, Rabah Mehaddi, Paul Lardet, Gilles Parent

► **To cite this version:**

Hassan Flity, Mariam Abdo, Lucas Terrei, Zoubir Acem, Rabah Mehaddi, et al.. 3D-Modeling of thermal degradation of spruce wood under inert atmosphere. *Fire Safety Journal*, 2023, 141, pp.103979. 10.1016/j.firesaf.2023.103979 . hal-04454738

HAL Id: hal-04454738

<https://hal.science/hal-04454738>

Submitted on 13 Feb 2024

HAL is a multi-disciplinary open access archive for the deposit and dissemination of scientific research documents, whether they are published or not. The documents may come from teaching and research institutions in France or abroad, or from public or private research centers.

L'archive ouverte pluridisciplinaire **HAL**, est destinée au dépôt et à la diffusion de documents scientifiques de niveau recherche, publiés ou non, émanant des établissements d'enseignement et de recherche français ou étrangers, des laboratoires publics ou privés.

3D-Modeling of thermal degradation of spruce wood under inert atmosphere

Hassan Flity^{a,b}, Mariam Abdo^{a,c}, Lucas Terrei^a, Zoubir Acem^a, Rabah Mehaddi^a, Paul Lardet^b, Gilles Parent^{a*}

^aUniversité de Lorraine, CNRS, LEMTA, F-54000 Nancy, France.

^bUniversité Paris-Est, CSTB, F-77447 Champs-sur-marne, France.

^cUniversité de Lorraine, INRAE, LERMAB, ERBE, F-88000 Epinal, France.

*Corresponding author: gilles.parent@univ-lorraine.fr

Highlights:

- Thermogravimetric analysis of wood.
- Experiments at the cone calorimeter using thermally inert material.
- 3D-Modeling of wood thermal degradation at the cone calorimeter scale.

Abstract:

The aim of this work was to model the thermal degradation of wood in an inert atmosphere at the cone calorimeter scale. First, the degradation of spruce wood was studied at the matter scale by TGA and DSC in an inert atmosphere at different heating rates. The kinetic parameters associated with a global multi-reaction mechanism were estimated by fitting the mass loss and the mass loss rate obtained by the TGA. The heats of reaction associated with the reaction scheme were estimated by fitting the heat flux measured by DSC. Then, experiments with an inert material (calcium silicate) were performed at the cone calorimeter scale under an inert atmosphere to characterize the boundary conditions of the developed 3D heat transfer model. The boundary conditions were determined by minimizing the difference between the measured in-depth temperatures and the predictions of the model using a least squares method. The results showed good predictions in agreement with experimental data and the convective heat transfer coefficients obtained were realistic. Finally, a 3D pyrolysis model, taking into account the anisotropic nature of wood, was developed by coupling the heat transfer with the kinetic model. The latter model was validated by comparison with tests carried out on spruce wood in an inert atmosphere using a cone heater.

Keywords: Wood; Thermal degradation; 3D-Pyrolysis model; Thermogravimetric analysis; Cone calorimeter

1. Introduction

Wood is a material with interesting thermal and mechanical properties and its carbon footprint is one of the lowest among building materials [1, 2]. Unfortunately, the fire behavior of wood limits its use in buildings [3]. A better understanding and control of the fundamental processes of wood combustion, in particular the primary pyrolysis phase, can help to reduce the constraints on the use of wood as a building material.

This topic is mainly studied at matter scale using TGA [4, 5, 6] under inert atmosphere. At this scale, the sample mass is very small (4 to 50 mg) and the sample is thermally thin, so heat transfer can be neglected and a 0D model can be used to predict the mass loss. Several mechanisms have been proposed in the literature to predict the mass loss and the mass loss rate obtained from TGA. These mechanisms can be divided into two

43 main categories. Some studies consider the wood as a homogeneous material for which
44 thermal degradation occurs according to a single step [7], consecutive steps [8], parallel
45 reactions [9] or a combination of parallel and consecutive reactions [10]. Other authors
46 consider that this description is not sufficient to predict the thermal degradation of wood,
47 which should rather be considered as the sum of the degradation of its main components:
48 hemicellulose, cellulose, lignin [11, 12]. Models of these two categories have advantages
49 and drawbacks: more or less complex, more or less predictive. However, the results of all
50 of them are satisfactory in 0D.

51 In the context of building fires, wood materials are thermally thick, requiring the study
52 of pyrolysis at larger scales. Today, the cone calorimeter is the largest scale at which
53 the thermal degradation is studied in an inert atmosphere [8, 13]. At this scale, heat
54 transfer controls the pyrolysis phenomena and must be taken into account. The multi-
55 scale approach is used to model the degradation at this scale *i.e.* the kinetic parameters
56 are estimated at 0D and used in a 1D or 3D model coupled with heat transfer. Several tools
57 can be used to model the thermal degradation of materials *e.g.* Fire Dynamic Simulator
58 (FDS), GPYRO [14], THERMAKIN [15]. Bustamante [16] showed the inadequacy of
59 FDS to simulate cone calorimeter tests with kinetic parameters calculated from TGA.
60 THERMAKIN cannot simulate 3D problems. Meanwhile, several studies have shown
61 the ability of GPYRO to simulate materials degradation at a large scale. However, in
62 GPYRO, thermal properties vary according to power laws and material properties are
63 calculated according to mixture laws. The latter assumption is true for some properties
64 such as the heat capacity, but it is not appropriate for the thermal conductivity. These
65 features are two significant weaknesses of GPYRO. It is worth mentioning the studies
66 conducted by Richter and Rein [17], as well as the study by Lautenberger and Fernandez-
67 Pello [18], who utilized the GPYRO model to simulate the pyrolysis and oxidation of
68 wood under three different oxygen concentrations: 0 %, 10.5 %, and 21 %. The models
69 were validated on the basis of the experimental results obtained by Kashiwagi *et. al* [13]
70 on samples of white pine, considering constant thermal properties. The results were quite
71 good and the remaining discrepancies were attributed to the uncertainty in the boundary
72 conditions, the material properties and their variation with temperature (in particular
73 the thermal diffusivity of wood and char) and the kinetic parameters of char oxidation.
74 It should be noted that Kashiwagi *et al*'s experiments [13] were performed on 3.8 cm side
75 cubic samples, so the heat transfer can hardly be considered 1D in this case, especially
76 for the in-depth temperature at locations far from the surface of the sample (temperature
77 was measured up to 15 mm deep).

78 The aim of this study was to simulate the thermal degradation of spruce wood at the
79 cone calorimeter scale in an inert atmosphere, following the work of Terrei *et al.* [8],
80 but now using measured wood thermal properties and an improved modeling including
81 in particular a 3D heat transfer (instead of 1D). First, wood was characterized at the
82 matter scale thanks to TGA tests as it is commonly done. These tests were carried out
83 at different heating rates. The kinetic parameters involved in a global multi-reaction
84 mechanism were estimated by fitting the mass loss and the mass loss rate obtained by
85 the TGA. More originally, DSC measurements were performed to determine the heats
86 of reaction corresponding to the different reactions taking place in the material during
87 its degradation. In a second step, tests were carried out at the material scale in inert
88 atmosphere using the cone calorimeter. At this scale, particular attention was paid to the
89 determination of the thermal boundary conditions. For this purpose, tests with an inert
90 material were carried out with the same experimental conditions as the wood tests. An

91 inverse method using a 3D heat transfer model was applied to these tests to determine
 92 the boundary conditions. Finally, a 3D pyrolysis model was developed in PYTHON
 93 to simulate wood degradation at the cone scale. The model accounts for the anisotropic
 94 nature of wood. The kinetic parameters obtained from TGA and the boundary conditions
 95 obtained from the inert material tests were used in the 3D pyrolysis model. In addition,
 96 all properties of the model were measured experimentally except the thermal conductivity
 97 above 200 °C. The latter property was varied until the best agreement between numerical
 98 and experimental results was obtained. Since the model used is complex and most of its
 99 parameters have been measured experimentally, the thermal conductivity obtained should
 100 be reliable.

101 2. Matter scale

102 The aim of this section is to present the thermal degradation of spruce wood at the matter
 103 scale. For this purpose, the degradation of spruce wood in an inert atmosphere has been
 104 studied by TGA and DSC. At this scale, the spatial temperature gradients within the
 105 wood sample are negligible, thus only the kinetics of the chemical reactions occurring
 106 during pyrolysis is involved.

107 2.1 Thermogravimetric analysis

108 Dry solid wood samples with an initial mass varying between 4.5 and 5 mg were subjected
 109 to a temperature ramp from room temperature to 1000 °C at different heating rates of 5,
 110 10 and 20 °C · min⁻¹. The tests were carried out under inert atmosphere using nitrogen
 111 with a flow rate of 80 mL · min⁻¹ to avoid oxidation of the char and thus concentrate on the
 112 sole pyrolysis. The evolution of the sample mass as a function of the sample temperature,
 113 was continuously recorded. Fig. 1 shows the mean normalized mass loss and the mean
 114 normalized mass loss rate as a function of temperature for the different heating rates. For
 115 each heating rate, three repeatability tests were performed with a relative difference of
 116 approximately 1.3 %.

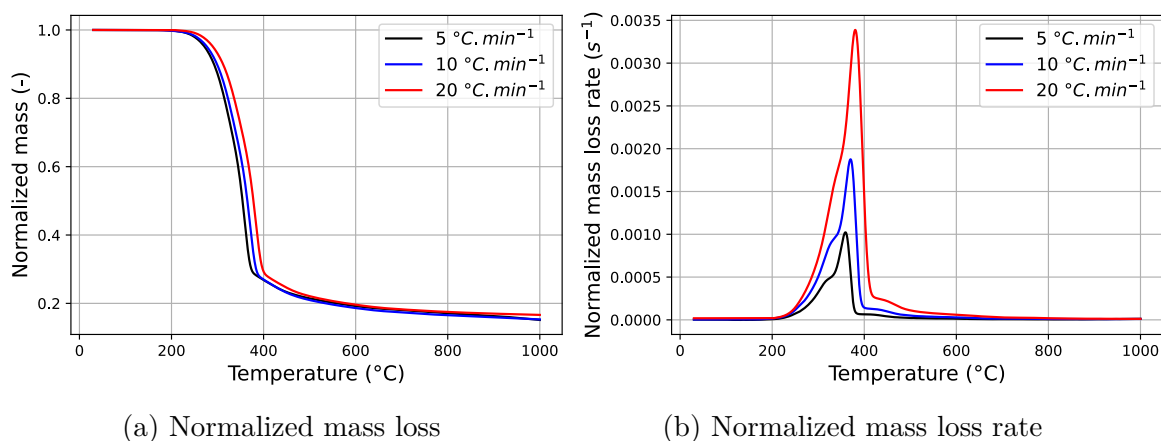


Fig. 1. Mean normalized mass loss and mean normalized mass loss rate as a function of temperature for the different heating rates: 5, 10 and 20 °C · min⁻¹.

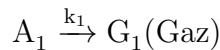
117 For a given heating rate, the observed stages of decomposition of the spruce wood are as
 118 follows:

- 119 - **Below 210 °C:** the mass of the samples remains constant.
- 120 - **At 210 °C:** the degradation of spruce begins and the mass of spruce starts to
121 decrease.
- 122 - **Between 300 °C and 350 °C:** there is a peak in the mass loss rate. This peak
123 corresponds mainly to the degradation of hemicellulose as reported in several studies
124 [6, 8, 11].
- 125 - **Between 350 °C and 420 °C:** the main step of degradation occurs and a signif-
126 icant peak in mass loss rate is observed. During this stage, the wood loses more
127 than 70 % of its initial mass. This step corresponds mainly to the degradation of
128 cellulose [6, 8, 11].
- 129 - **After 420 °C:** the mass loss rate decreases slightly until a plateau is reached. This
130 is due to the degradation of a part of the lignin. In fact, lignin degradation occurs
131 over a wide temperature range, from 200 °C to 900 °C [19, 20].

132 Overall, the experimental results show that wood degradation follows the same trend
133 regardless of the heating rate. However, Fig. 1 (b) shows a strong influence of the heating
134 rate on the intensities of the mass loss rate peaks. Thus, the higher the heating rate,
135 the higher the maximum mass loss rate. Fig. 1 (b) also shows that as the heating rate
136 increases, the different mass loss rate peaks occur at higher temperatures. This behavior
137 has also been observed in several studies [10, 11]. Indeed, when the heating rate is low,
138 the temperature within the sample increases uniformly. On the other hand, when the
139 heating rate is high, the temperature within the sample is no longer uniform and the
140 temperature in the core of the wood is not exactly that of the reactor [12].

141 2.2 Kinetic model

142 Based on the experimental results, the model used to predict the wood degradation is
143 a global multi-reaction model. In this model, dry wood is considered to be composed
144 of three pseudo-solids A_1 , A_2 and A_3 , with initial mass fractions equal to α_1 , α_2 and
145 α_3 respectively. These pseudo-components degrade simultaneously and independently
146 according to first-order kinetic laws. A_1 degradation only leads to a gaseous constituent
147 G_1 , the decomposition of A_2 leads to a gaseous constituent G_2 and a char constituent C_2 .
148 The decomposition of A_3 leads to a gaseous constituent G_3 and a char constituent C_3 .
149 Further details of this model and the theory behind it will be published in a future paper
150 which is currently under review. The reaction scheme adopted is therefore as follows:



153 Where: γ_2 and γ_3 are the stoichiometric coefficients. K_1 , K_2 and K_3 are the rate coeffi-
154 cients of the reactions which follow an Arrhenius law ($K_i = K_{0i} \cdot \exp(-E_i/RT)$). K_{0i} and E_i
155 are the pre-exponential factor and the activation energy of the reaction i , respectively, T

156 is the temperature and R is the ideal gas constant. The mass balance of A_1 , A_2 , A_3 , C_2
 157 and C_3 are respectively:

$$\frac{dm_{A_1}}{dt} = -K_1 \cdot m_{A_1} \quad (1)$$

$$\frac{dm_{A_2}}{dt} = -K_2 \cdot m_{A_2} \quad (2)$$

$$\frac{dm_{A_3}}{dt} = -K_3 \cdot m_{A_3} \quad (3)$$

$$\frac{dm_{C_2}}{dt} = \gamma_2 \cdot K_2 \cdot m_{A_2} \quad (4)$$

$$\frac{dm_{C_3}}{dt} = \gamma_3 \cdot K_3 \cdot m_{A_3} \quad (5)$$

162 Where m_{A_1} , m_{A_2} , m_{A_3} , m_{C_2} and m_{C_3} are respectively the mass of the components A_1 ,
 163 A_2 , A_3 , C_2 and C_3 . Eqs. 1, 2, 3, 4 and 5 were solved numerically to determine the mass
 164 of each component at the time t. Then, the total mass of the sample M(t) is calculated
 165 by:

$$M(t) = m_{A_1}(t) + m_{A_2}(t) + m_{A_3}(t) + m_{C_2}(t) + m_{C_3}(t) \quad (6)$$

166 The kinetic parameters of the model *i.e.* pre-exponential factors (K_{01} , K_{02} and K_{03}),
 167 activation energies (E_1 , E_2 and E_3) and stoichiometric coefficients (α_1 , α_2 , α_3 , γ_2 and γ_3)
 168 were estimated by simultaneously fitting the mass loss and the mass loss rate curves ob-
 169 tained by TGA. Levenberg-Marquardt algorithm [21] was used to minimize the following
 170 objective function:

$$S = \sum_{i=1}^N [M_{exp}(t_i) - M_{mod}(t_i)]^2 + \delta \sum_{i=1}^N \left[\frac{dM_{exp}}{dt}(t_i) - \frac{dM_{mod}}{dt}(t_i) \right]^2 \quad (7)$$

171 Where: N is the number of experimental points; $M_{exp}(t_i)$ and $\frac{dM_{exp}}{dt}(t_i)$ are the mea-
 172 sured mass and mass loss rate, respectively; $M_{mod}(t_i)$ and $\frac{dM_{mod}}{dt}(t_i)$ are the corresponding
 173 numerical quantities. As the magnitude of the mass loss is extremely higher than the
 174 mass loss rate, the sum of the mass loss rate is multiplied by a factor (δ) to increase the
 175 weight of the mass loss rate in the optimization. Several constraints were applied on the
 176 parameters during the optimization. Firstly, as there is a compensation effect between
 177 the pre-exponential factor and the activation energy [22], the algorithm could converge
 178 toward different sets of parameters. Thus, the activation energy was constrained to vary
 179 between 60 and 200 $\text{kJ} \cdot \text{mol}^{-1}$ which is the order of magnitude of this parameter in the
 180 literature. Table 1 shows the values of the kinetic parameters obtained by optimization.
 181 Fig. 2 shows that the model generally well predicts the normalized mass loss and the
 182 normalized mass loss rate obtained by TGA. A slight discrepancy is observed above 400
 183 $^{\circ}\text{C}$. This can be attributed to a delayed degradation of the third component A_3 . In addi-
 184 tion, this kinetic mechanism, with only three first order reactions, can be considered too
 185 simple to account for all the reactions that occur at high temperature.

186 2.3 Differential scanning calorimetry

187 The differential scanning calorimeter used in this study is the SETARAM DSC 111.
 188 This instrument has been modified and equipped with an original fixed-bed setup to
 189 ensure better control of sample scanning. Prior to performing the tests, the instrument

Table 1. The kinetic parameters obtained by optimisation.

Reaction	K_{0i} (s^{-1})	E_i ($kJ \cdot mol^{-1}$)	α_i (-)	γ_i (-)
(1)	7.1×10^8	123	0.17	-
(2)	1.3×10^{12}	173	0.61	0.1
(3)	552	81	0.22	0.59

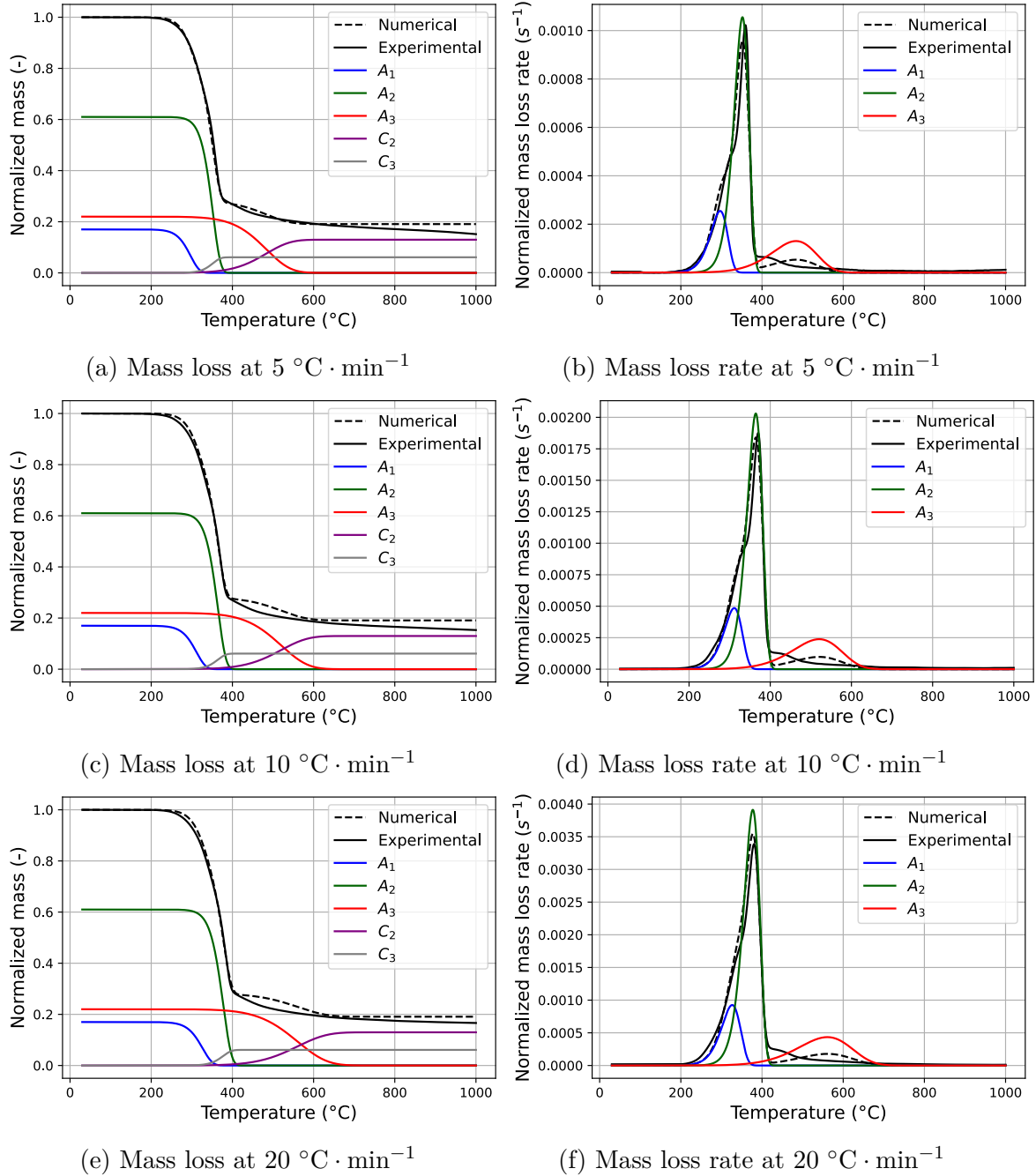


Fig. 2. Comparison between the numerical and experimental results for different heating rates. A_1 , A_2 , and A_3 are the pseudo-components of wood, while C_2 and C_3 are two char constituents.

190 was calibrated (temperature and sensitivity) using the melting temperature and enthalpy

191 of the following standard materials: indium, tin, lead and zinc. The calibration was
 192 performed under the same experimental conditions as the wood tests, i.e., the same heating
 193 rate, argon flow rate, and temperature program. Prior to each wood test, an empty tube
 194 test was performed to establish the baseline of the apparatus. The tests were performed
 195 at a heating rate of $10 \text{ K} \cdot \text{min}^{-1}$, ranging from room temperature to $600 \text{ }^\circ\text{C}$, under an
 196 inert atmosphere using nitrogen at a flow rate of $20 \text{ mL} \cdot \text{min}^{-1}$. The samples tested were
 197 cylindrical with a diameter of 3.4 mm and a height of 6.5 mm . These samples were oven
 198 dried at 105°C for 24 hours prior to testing. Note that Q_{total}^{exp} is the heat flux measured
 199 by the DSC, corrected by the instrument baseline and normalized by the initial mass of
 200 the sample and the heating rate. Q_{total}^{exp} was assumed to be the sum of an effective heat
 201 capacity (sensible heat flux Q_s) and the heat of reaction Q_r . The effective heat capacity
 202 is assumed to be as follows [23]:

$$C_p(T) = (1 - X(T)) \cdot C_{p,wood}(T) + X(T) \cdot C_{p,char}(T) \cdot (\gamma_2 + \gamma_3) \quad (8)$$

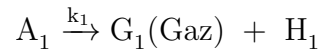
203 Where: $(\gamma_2 + \gamma_3)$ is the final char yield, $C_{p,wood}(T)$ is the heat capacity of wood, $C_{p,char}(T)$
 204 is the heat capacity of char and $X(T)$ is the mass conversion defined by:

$$X(T) = \frac{m_0 - m(T)}{m_0 - (\gamma_2 + \gamma_3)} \quad (9)$$

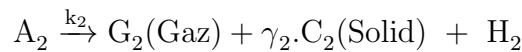
205 Where m_0 and $m(T)$ are the initial mass and the mass of the sample at the temperature
 206 T calculated from the kinetic model, respectively. Therefore, the normalized heat flux
 207 measured by DSC can be modeled as:

$$Q_{total}^{num}(T) = \overbrace{(1 - X(T))C_{p,wood}(T) + X(T)C_{p,char}(T)(\gamma_2 + \gamma_3)}^{\text{Effective heat capacity } (C_p(T))} + \frac{1}{\beta} \overbrace{\left(\sum_{i=1}^3 \frac{\frac{dm_{A_i}(T) H_i}{dt}}{\alpha_i} \right)}^{\text{Heat of reactions } (Q_r)} \quad (10)$$

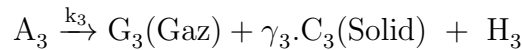
208 Where: H_i is the heat of reaction i , and β is the heating rate. Finally, the heats of
 209 reactions H_1 , H_2 , and H_3 were estimated by minimizing the sum of the quadratic error
 210 between Q_{total}^{num} and Q_{total}^{exp} . Fig. 3 (a) shows that the three reactions used to predict the
 211 mass loss at the macro scale were unable to predict the heat flux measured by DSC.
 212 Therefore, a fourth reaction was added, and the reaction scheme became as follows:



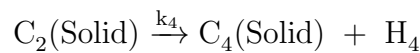
213



214



215



216 Where H_1 , H_2 , H_3 , and H_4 are the respective heats of reaction 1, 2, 3, and 4. Note that in
 217 the fourth reaction, there is only heat production and no mass loss. In this reaction, the
 218 char C_2 is converted into another char C_4 with the same mass but a different morphology.
 219 In this case, the heat of reactions Q_r in Eq. 10 becomes:

$$Q_r = \frac{1}{\beta} \left(\sum_{i=1}^3 \frac{\frac{dm_{A_i} H_i}{dt}}{\alpha_i} + \frac{\frac{dm_{C_2} H_4}{dt}}{\alpha_2 \gamma_2} \right) \quad (11)$$

220 Fig. 3 (b) shows that the kinetic scheme with 4 reactions predicts the experimental
 221 data very well. The following heats of reaction were obtained: $H_1 = -37.5\text{kJ} \cdot \text{kg}^{-1}$,
 222 $H_2 = 124.6\text{kJ} \cdot \text{kg}^{-1}$, $H_3 = 0$, and $H_4 = -88\text{kJ} \cdot \text{kg}^{-1}$. The kinetic parameters for the
 223 fourth reaction are: $K_{04} = 1.1 \times 10^5\text{s}^{-1}$ and $E_4 = 100\text{kJ} \cdot \text{mol}^{-1}$. The kinetic parameters
 of reactions (1), (2), and (3) remain the same as the parameters presented in Table 1.

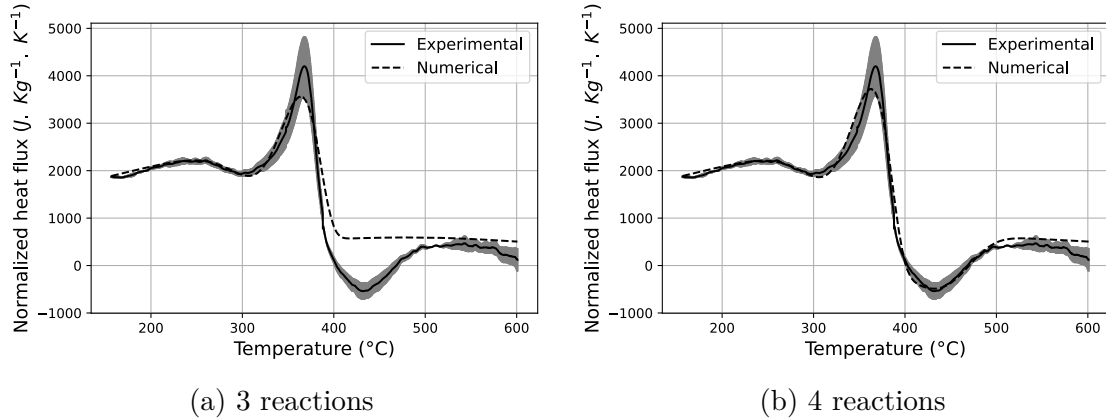


Fig. 3. Comparison between the normalized heat flux measured by DSC and the numerical heat flux predicted with the model using (a) 3 reactions and (b) 4 reactions. The experimental data is the average of three repeatability tests.

224

225 3. Cone calorimeter scale

226 This section is dedicated to the study of spruce wood degradation under inert atmosphere
 227 at the cone calorimeter scale. At this scale, heat transfer cannot be neglected.

228 3.1 Materials and methods

229 The aim of this work was to model the thermal degradation of spruce wood in an inert
 230 atmosphere at the cone calorimeter scale, following the work of Terrei *et al.* [8]. These
 231 authors carried out cone calorimeter experiments with spruce wood samples (0.1×0.1
 232 $\times 0.05 \text{ m}^3$) oriented vertically. During the tests, the samples were placed in a stainless-
 233 steel chamber. Continuous argon injection at a low flow rate maintained an oxygen
 234 concentration less than 3 % inside the chamber to prevent char oxidation. The sides and
 235 rear of the chamber were cooled down by water heat exchangers. The heat flux coming
 236 from the cone passes through a sapphire window placed on the front face of the chamber.
 237 Wood samples were placed in a calcium silicate sample holder (3 cm thick) to reduce
 238 lateral convection losses. The mass loss of the samples was measured by a weighing scale
 239 with 0.01 g accuracy. Twelve K-type 0.1 mm diameter thermocouples were embedded in
 240 the samples at different depths (2, 4, 6, 8, 10, 12, 14, 16, 18, 20, 30 and 40 mm), along
 241 the centerline of the samples, following the technique developed in Terrei *et al.*'s study
 242 [24]. Tests were performed at 35 and 45 $\text{kW} \cdot \text{m}^{-2}$. Further details about the experimental
 243 protocol can be found in [8].

244 Since several physical and chemical phenomena occur during wood experiments, it is
 245 difficult to characterize the thermal boundary conditions for the sample inside a chamber,
 246 in particular considering that the sapphire window is heated up during the experiment.
 247 Therefore, tests with an inert material were performed inside the chamber under the same

248 conditions as the wood tests *i.e.* same heat fluxes, argon flow rate and sample holder. In
 249 this case, only heat transfer occurs and it is easier to characterize the boundary conditions
 250 such as convection and radiative heat losses. The chosen inert material was low density
 251 calcium silicate (Silcal 1100[®]) since its thermal properties are close to those of spruce wood:
 252 the specific heat is around $1000 \text{ J} \cdot \text{kg}^{-1} \cdot \text{K}^{-1}$ and the thermal conductivity varies between
 253 0.08 and $0.2 \text{ W} \cdot \text{m}^{-1} \cdot \text{K}^{-1}$ depending on the temperature [25]. Twelve thermocouples
 254 were also embedded along the centerline of the calcium silicate sample at the same depths
 255 as the wood samples. Moreover, an additional thermocouple was fixed at the rear face of
 256 the sample.

257 3.2 3D heat transfer model and estimation of the boundary conditions

258 A 3D heat transfer model was developed in PYTHON environment. The heat transfer
 259 balance described by eq. 12 was numerically solved using a finite volume method. For
 260 temporal discretization, an explicit scheme was used.

$$\rho C_p(T) \frac{\partial T}{\partial t} = \nabla \cdot (\bar{\lambda}_c(T) \nabla T) \quad (12)$$

261 $\bar{\lambda}_c$ is the thermal conductivity tensor. For calcium silicate, it reduces to a scalar because
 262 it is isotropic, but this will not be the case for wood. The boundary conditions are
 given in Fig. 4. Where: h_{front} and h_{lateral} are the convective heat transfer coefficients for

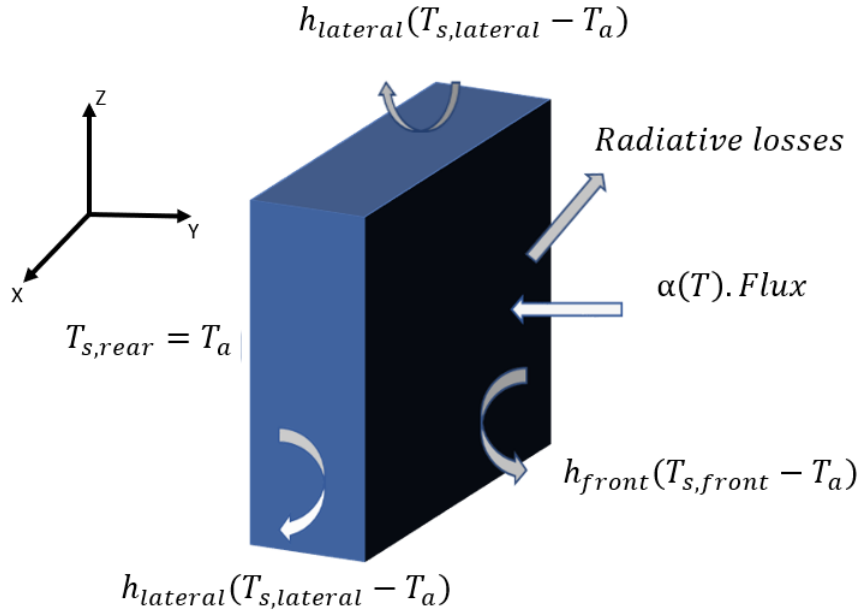


Fig. 4. Boundary conditions of a sample exposed to the cone calorimeter.

263 respectively the front and the lateral faces. $T_{S,\text{front}}$, $T_{S,\text{rear}}$ and $T_{S,\text{lateral}}$ are the surface
 264 temperature for respectively the front, the rear and the four lateral faces. $\alpha(T)$ is the
 265 absorptivity. T_a is the temperature of the atmosphere inside the steel chamber, assumed
 266 to be equal to the temperature measured at the back of the sample. Radiative losses
 267 depend on the radiative heat flux exchanged between the front of the sample and the
 268 sapphire window. Sapphire is a non grey and semi transparent material. Its spectral
 269 reflectivity $R(\lambda)$ (λ being the wavelength) and transmissivity ($\text{Tr}(\lambda)$) were measured using
 270

271 a Fourier Transform Infrared (FTIR) Spectrometer. Calcium silicate is considered to be
 272 a non grey and opaque material. Its spectral reflectivity was also measured using FTIR
 273 spectroscopy. Absorptivity and emissivity were obtained from the radiative energy balance
 274 *i.e.* $\alpha(\lambda) = 1 - \text{Tr}(\lambda) - R(\lambda)$ and Kirchoff law ($\epsilon(\lambda) = \alpha(\lambda)$). The sample radiative
 275 losses are thus modelled as

$$\phi = \pi \int \left[\frac{\epsilon_1(\lambda)\epsilon_2(\lambda)}{\epsilon_1(\lambda) + \epsilon_2(\lambda) - \epsilon_1(\lambda)\epsilon_2(\lambda)} (I_\lambda^{bb}(T_1) - I_\lambda^{bb}(T_2)) - \text{Tr}_1(\lambda)\epsilon_2(\lambda)I_\lambda^{bb}(T_2) \right] d\lambda \quad (13)$$

276 subscript 1 refers to the sapphire and subscript 2 to the sample (here the calcium silicate).
 277 $I_\lambda^{bb}(T)$ is the blackbody intensity (Planck function). The first term corresponds to the
 278 radiative heat exchange between the sapphire surface and the sample (if sapphire is hotter
 279 than the sample, this term is positive and corresponds to an energy gain, otherwise it is
 280 negative and it is an energy loss). The second term corresponds to the radiative heat flux
 281 emitted by the sample and transmitted through the sapphire window. The integral has
 282 been approximated by the rectangular method with a $\Delta\lambda = 0.2 \mu\text{m}$ interval.

283 The temperature of the sapphire window was measured as a function of the exposure
 284 time (the sapphire window is heated up during the experiment) by an infrared camera
 285 (FLIR SC7300 LW) equipped with a $7.9 \mu\text{m}$ optical bandpass filter. At this wavelength
 286 sapphire is opaque and almost black (0.98 emissivity). The radiation emitted by the cone
 287 and reflected by the sapphire surface was subtracted from the measured radiation to only
 288 measure the radiation emitted by the sapphire window, following the procedure described
 289 in [26].

290 The heat capacity of the calcium silicate was measured as a function of temperature in
 291 [25] and was found to be equal to: $C_p(T) = 439 + 83 \log_{10}(T + 273)$ where T is the tem-
 292 perature in °C. The density of calcium silicate was measured and found to be $240 \text{ kg} \cdot \text{m}^{-3}$.
 293 The thermal conductivity (λ_c) was assumed to vary with the temperature according to a
 294 second degree polynomial:

$$\lambda_c(T) = \lambda_{c1}T^2 + \lambda_{c2}T + \lambda_{c3} \quad (14)$$

296 Where λ_{c1} , λ_{c2} and λ_{c3} are three constants to be estimated. An inverse method was applied
 297 on the temperature measurements obtained from the inert atmosphere calcium silicate
 298 tests at 35 and $45 \text{ kW} \cdot \text{m}^{-2}$ using this model to characterize the boundary conditions.
 299 The objective function described by eq. 15 was minimized using the Levenberg-Marquardt
 300 algorithm.

$$S = \sum_{i=1}^N [T_{exp}(t_i) - T_{mod}(t_i)]^2 \quad (15)$$

301 Where: N is the number of experimental points, $T_{exp}(t_i)$ and $T_{mod}(t_i)$ are respectively the
 302 measured temperature and the temperature calculated by the 3D heat transfer model. The
 303 minimization was performed using the two heat fluxes simultaneously to estimate h_{front}
 304 and the thermal conductivity of the calcium silicate. Although the thermal conductivity
 305 of the calcium silicate was measured as function of temperature in Jannot *et al.*'s study
 306 [25], this property was kept as unknown in order to check the reliability of the parameters
 307 obtained by optimisation. Thus, an estimated thermal conductivity by inverse method
 308 close to the thermal conductivity measured experimentally by the hot wire technique [25]
 309 indicates that the convective heat transfer coefficient obtained by optimisation is reliable.
 310 $h_{lateral}$ was supposed to be equal to $10 \text{ W} \cdot \text{m}^{-2} \cdot \text{K}^{-1}$. In fact, a sensitivity analysis showed

311 that the measured temperatures are not sensitive to h_{lateral} , which makes sense because of
 312 the insulating role of the calcium silicate sample holder. It is therefore not possible to
 313 estimate this parameter by inverse method.

314 **3.3 3D pyrolysis model and thermo-physical properties of wood**

315 The 3D heat transfer model was coupled with the kinetic model in order to predict the
 316 thermal degradation of spruce wood in an inert atmosphere at the cone calorimeter scale.
 317 The following assumptions were made for the 3D pyrolysis model:

- 318 - Heat and mass transfer in the gas phase were not considered in the model.
- 319 - Effect of shrinking, cracking and swelling were neglected.

320 The degradation of wood occurs following the kinetic scheme presented in the matter scale
 321 section. The heat capacity of spruce wood was measured between 30 and 100 °C in 10 °C
 322 increments using a DSC SETARAM microDSC3 instrument. The heat capacity obtained
 323 is $C_{p,wood}(T) = 1131 + 4.67T$ where T is in °C. The latter correlation was extrapolated for
 324 the higher temperatures. The heat capacity of char was also measured between 30 and
 325 600 °C and the heat capacity obtained is $C_{p,char}(T) = 693 + 3.44T$. The effective heat
 326 capacity was calculated as in equation 8. More details on the measurement technique of
 327 the heat capacity will be published in a future paper. Therefore, the energy conservation
 328 equation is as follow:

$$\frac{\partial}{\partial t}(\rho \cdot C_p \cdot T) = \nabla \cdot (\bar{\lambda}_c(T) \nabla T) + k_1 \cdot \rho_1 \cdot H_1 + k_2 \cdot \rho_2 \cdot H_2 + k_3 \cdot \rho_3 \cdot H_3 + k_4 \cdot \rho_{C_2} \cdot H_4 \quad (16)$$

329 Where: ρ is the bulk density calculated by $\rho = \rho_1 + \rho_2 + \rho_3 + \rho_{C_2} + \rho_{C_3} + \rho_{C_4}$; ρ_1 , ρ_2 ,
 330 ρ_3 , ρ_{C_2} , ρ_{C_3} and ρ_{C_4} are the mass of respectively the constituents A_1 , A_2 , A_3 , C_2 , C_3
 331 and C_4 per unit volume. The thermal boundary conditions are given in Fig. 4 and the
 332 convective heat transfer coefficients are those estimated from the calcium silicate tests.
 333 The emissivity of the sample surface was measured as a function of the exposure time to
 334 the cone heater [8]. In the present model, the mean of the latter measurements was used
 335 *i.e.* 0.9 and the absorptivity was considered equal to the emissivity, since wood is almost
 336 grey and the surface chars quite rapidly, and char is even greyer than wood. The thermal
 337 conductivity of spruce wood was measured between 30 and 160 °C in the two directions
 338 parallel and perpendicular to the fiber direction [27] using the anisotropic parallel hot wire
 339 technique [28]. The latter measurements show that the transverse thermal conductivity
 340 increase from $0.096 \text{ W} \cdot \text{m}^{-1} \cdot \text{K}^{-1}$ at 20 °C to $0.110 \text{ W} \cdot \text{m}^{-1} \cdot \text{K}^{-1}$ at 160 °C. Meanwhile,
 341 the longitudinal thermal conductivity was found to be almost independent of temperature
 342 and equal to $0.345 \text{ W} \cdot \text{m}^{-1} \cdot \text{K}^{-1}$. It is worth noting that several studies have shown that
 343 the radial and tangential thermal conductivity of wood are similar [29, 30, 31, 32, 33].
 344 Therefore, the thermal conductivities used in the model below the onset of pyrolysis were
 345 $\lambda_{c\perp} = 0.102 \text{ W} \cdot \text{m}^{-1} \cdot \text{K}^{-1}$ in the transverse direction (radial and tangential) and $\lambda_{c\parallel}$
 346 $= 0.345 \text{ W} \cdot \text{m}^{-1} \cdot \text{K}^{-1}$ in the longitudinal direction. Above 200 °C, the model assumes
 347 that the longitudinal thermal conductivity remains constant and the transverse thermal
 348 conductivity depends only on temperature according to the following law:

$$\lambda_{c\perp} = 0.102 + \lambda_1 \cdot (T - 200) + \lambda_2 \cdot (T - 200)^2 \quad (17)$$

349 Where T is the temperature in °C, λ_1 and λ_2 were chosen in order to give a calculated
 350 mass loss, a calculated mass loss rate and calculated in-depth temperatures similar to

351 those obtained from the cone calorimeter tests on spruce under inert atmosphere. The
 352 thermal conductivity tensor is therefore

$$\bar{\lambda}_c = \begin{pmatrix} \lambda_{c\perp} & 0 & 0 \\ 0 & \lambda_{c\perp} & 0 \\ 0 & 0 & \lambda_{c\parallel} \end{pmatrix} \quad (18)$$

353 x -axis is horizontal parallel to the exposed surface, y -axis is parallel to the cone heat flux
 354 and z -axis is vertical (thus wood fibers are oriented vertically), as shown in Fig. 4.
 355 Finally, a perfect thermal contact was considered between the wood sample and the
 356 calcium silicate sample holder and the thermal properties of the latter material were
 357 taken from the work of Jannot *et al.* [25].

358 4. Results and discussion

359 4.1 Calcium silicate tests for estimation of boundary conditions

360 Fig. 5 shows the experimental in-depth temperatures at 35 and 45 kW · m⁻² and their
 361 comparison with the numerical temperatures.

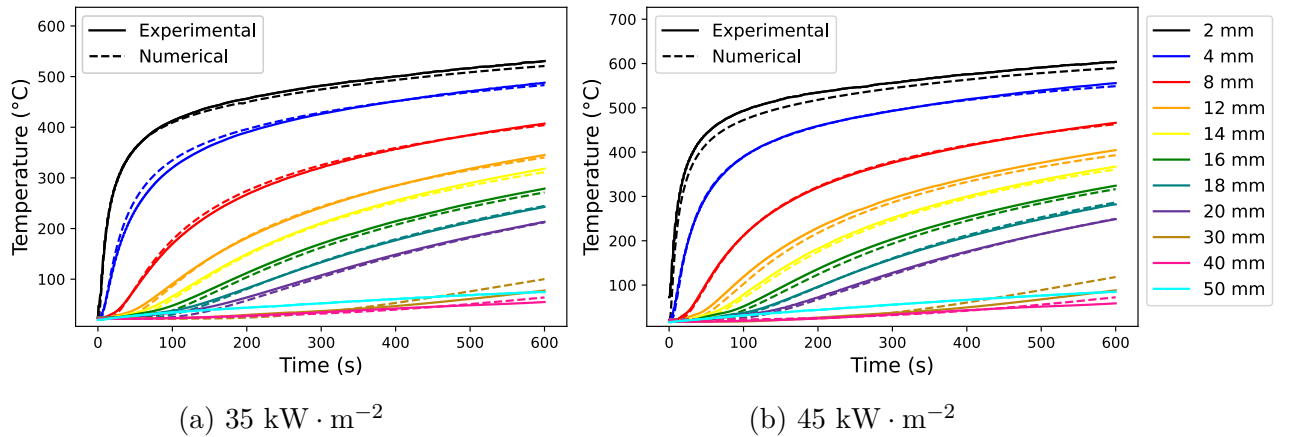


Fig. 5. Comparison between numerical and experimental in-depth temperature within the calcium silicate sample at two different heat fluxes.

362 The temperature measured at the rear face of the sample (50 mm) is higher than the
 363 temperature at 40 mm depth at the beginning of the test, indicating that the atmosphere
 364 inside the chamber is heated during the tests. The numerical and the experimental tem-
 365 peratures are in good agreement. The root-mean-square error obtained simultaneously
 366 for the two tests is 7 °C and the normalized root-mean-square error (NRMSE) is approx-
 367 imately 1.2 %. Fig. 6 shows the comparison between the estimated thermal conductivity
 368 and the thermal conductivity measured by the hot wire technique [25]. The two con-
 369 ductivities look very similar, almost linear with temperature, same slope, there is only a
 370 slight shift between them. The mean deviation between the estimated and the measured
 371 thermal conductivity is approximately 11.6 %. This is satisfactory considering i) the tem-
 372 perature measurement uncertainties (thermocouple accuracy and thermocouple position
 373 uncertainty), ii) that the inherent uncertainty of the hot wire technique used to measure
 374 the thermal conductivity is about 10 % [25] and iii) that the heat flux applied to the front
 375 of the sample was assumed to be homogeneous (which is not exactly the case¹). This is

¹consideration of a non-uniform heat flux will be investigated in the near future

376 very reassuring for the reliability of the results. The convective heat transfer coefficient
 377 obtained is $h_{front} = 31 \text{ W} \cdot \text{m}^{-2} \cdot \text{K}^{-1}$.

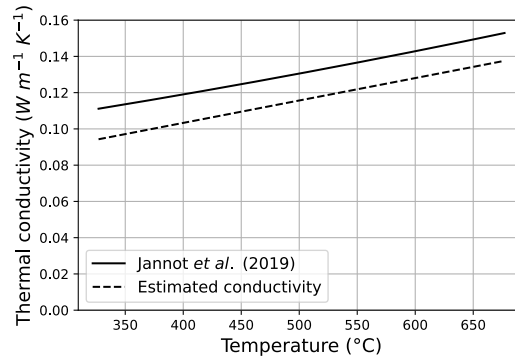


Fig. 6. Comparison between the estimated and the measured thermal conductivity of the calcium silicate [25].

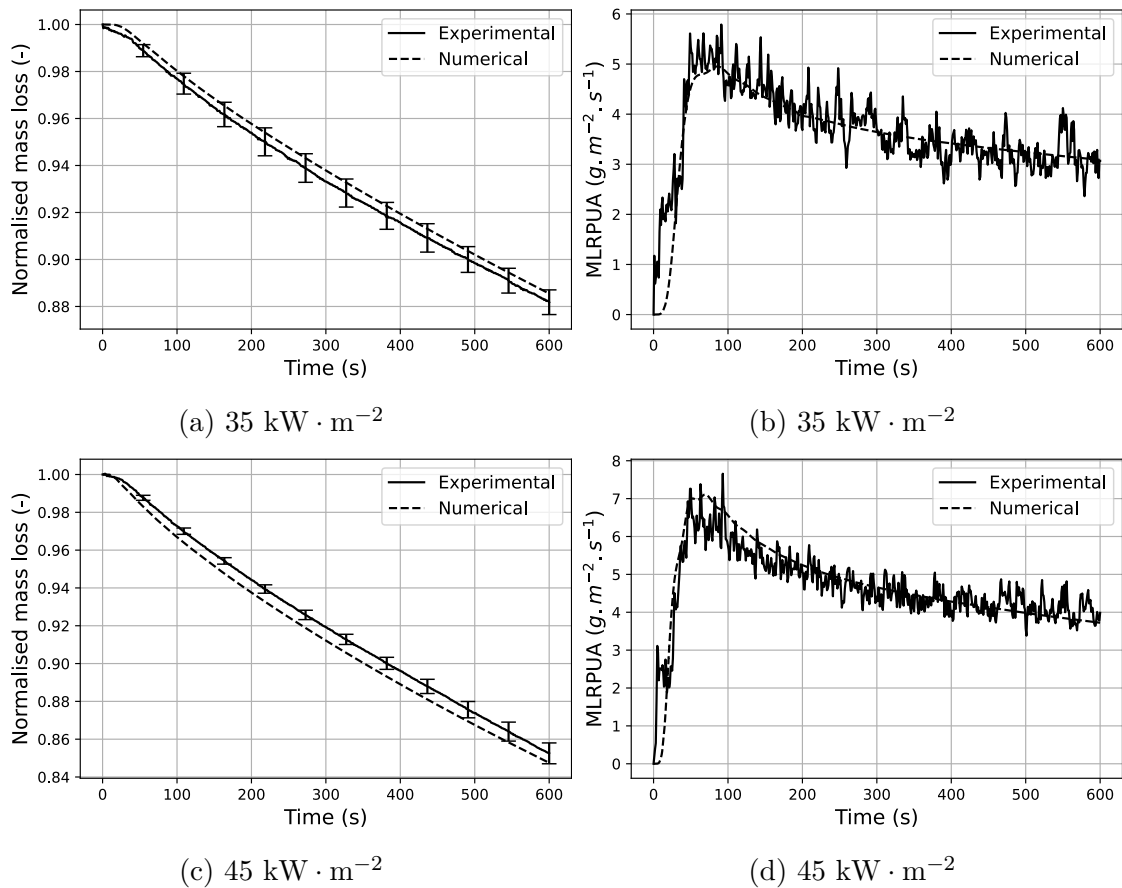


Fig. 7. Comparison between numerical and experimental mass loss and MLRPUA for wood tests at different heat fluxes.

378 4.2 Wood degradation at the cone calorimeter scale

379 As shown in the section 4.1, all properties of wood and calcium silicate were measured
 380 except thermal conductivity of wood/char above 200 °C. In addition, the boundary con-
 381 ditions were estimated from experiments with an inert material. Probably the convective

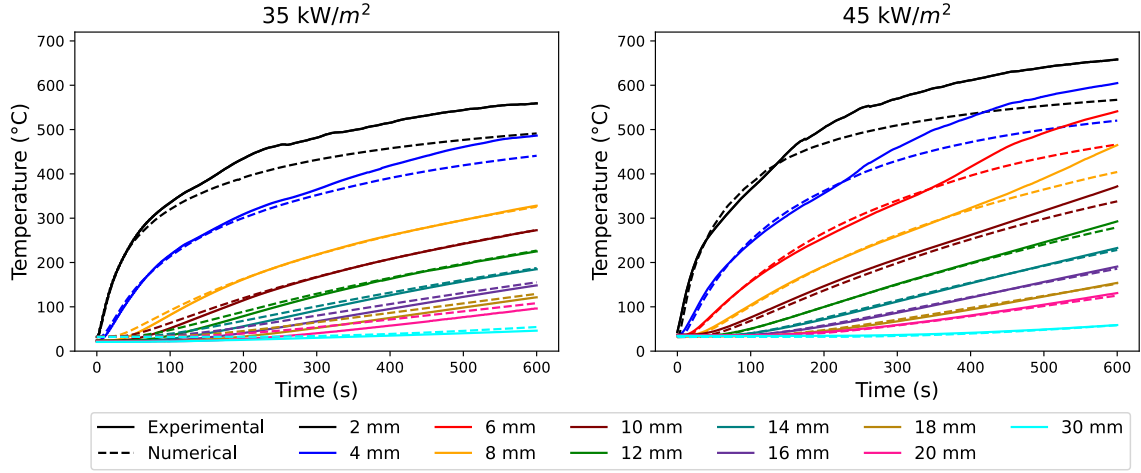


Fig. 8. Comparison between numerical and experimental in-depth temperature within the wood samples at different heat fluxes.

382 heat transfer coefficient could vary between calcium silicate and wood experiments, es-
 383 pecially for the face exposed to the cone calorimeter. However, at least the order of
 384 magnitude of the convection losses was obtained. Several simulations were carried out by
 385 varying the thermal conductivity of wood above 200 °C. The thermal conductivity that
 386 gave the better agreement with the experimental mass loss and the mass loss per unit
 387 area (MLRPUA) is as follows:

$$\lambda_{c\perp} = 0.102 + 8.1 \times 10^{-7} \cdot (T - 200)^2 \quad (19)$$

388 Where T is in °C. Fig. 7 shows the comparison between experimental and numerical
 389 MLRPUA at heat fluxes 35 and 45 kW · m⁻². Concerning mass loss, the normalized root
 390 mean squared error (NRMSE) obtained between numerical and experimental results is
 391 respectively 3.2 and 4.2 %. Meanwhile, the NRMSE obtained between numerical and ex-
 392 perimental MLRPUA is 6 and 5.6 % at respectively 35 and 45 kW · m⁻². All these results
 393 show the robustness of the numerical model to evaluate the mass loss and the MLRPUA
 394 at different heat fluxes.

395 Fig. 8 shows the comparison between numerical and experimental in-depth temperatures
 396 for the two heat fluxes. Below 400 °C, numerical and experimental temperatures comply
 397 very well. However, above 400 °C the pyrolysis model underestimates the temperature.
 398 It is interesting to note that the TGA analysis showed that spruce wood loses more than
 399 75 % of its initial weight between 200 and 400 °C *i.e.* more than 89 % of the degradation
 400 was already occurred below this temperature. Therefore, although there is a bias between
 401 experimental and numerical in-depth temperature at high temperatures, the model pre-
 402 dicts the mass loss and MLRPUA well at the different heating fluxes. The discrepancy
 403 between numerical and experimental temperatures at high temperatures could be caused
 404 by several reasons. Firstly, at high temperatures the wood turns to char, its porosity
 405 becomes very high and consequently the thermocouple is no longer in good contact with
 406 the material. The second reason is that the model considers a homogeneous medium,
 407 whereas when wood chars, cracks appear and the model no longer applies. Finally, the
 408 main reason is that although the atmosphere was inerted, smoldering combustion, *i.e.*
 409 char oxidation, can occur at a low rate because the oxygen content was not exactly zero.
 410 However, temperature and MLR predictions obtained with the model proposed in this
 411 paper have been significantly improved compared to our previous work [8].

412 5. Conclusion

413 In this work, a 3D heat transfer and pyrolysis model for spruce wood was developed at the
414 cone calorimeter scale under inert atmosphere. First, the thermal degradation of spruce
415 wood was studied by TGA under inert atmosphere between ambient temperature and
416 1000 °C at different heating rates (5, 10 and 20 K · min⁻¹). A global three-reaction mech-
417 anism was used to predict the mass loss and the mass loss rate. The kinetic parameters
418 were estimated by fitting TGA data. The numerical and experimental results were in
419 good agreement at this scale, where the wood sample is thermally thin and temperature
420 gradients are negligible. Moreover, DSC measurements were carried out under an inert
421 atmosphere at a heating rate of 10 K · min⁻¹. It was found that the kinetic scheme with
422 three reactions is unable to predict the heat flux measured by DSC. A fourth reaction
423 was therefore added. Based on the DSC and ATG measurements, as well as previous
424 measurements of the heat capacity of wood and char, the heat of pyrolysis of spruce wood
425 was modeled as a function of temperature. At a larger scale, cone calorimeter tests were
426 then carried out with an inert material in an inert atmosphere at 35 and 45 kW · m⁻².
427 The aim was to characterize the heat transfer boundary conditions for tests performed
428 on wood samples under the same conditions. An inverse method was applied to the in-
429 depth temperatures within a low density calcium silicate sample using a 3D heat transfer
430 model to estimate the convective heat coefficients and thermal conductivity of that sam-
431 ple. The results showed that the thermal conductivity of calcium silicate obtained by
432 optimization was in good agreement with the thermal conductivity measured by the hot
433 wire technique. Therefore, the other parameters obtained from optimization, such as the
434 convective heat transfer coefficient, can be considered reliable. Finally, a 3D pyrolysis
435 model was developed by coupling the kinetic model, whose parameters were obtained
436 from TGA, with a 3D heat transfer model. The boundary conditions estimated from the
437 calcium silicate tests were fixed. All properties of wood were measured experimentally
438 such as emissivity, absorptivity, heat capacity of wood until 100 °C, heat capacity of char
439 until 600 °C, thermal conductivity in transverse and longitudinal direction until 160 °C.
440 The heats of reaction were also determined using the DSC technique. The only property
441 that remained unknown was the thermal conductivity above 200 °C. This latter property
442 was varied until a good fit was obtained between the numerical mass loss, mass loss rate
443 and in-depth temperatures and their experimental counterparts. The results obtained
444 with the 3D pyrolysis model developed and presented in this work comply very satisfac-
445 torily with the experimental results and the thermal conductivity obtained above 200 °C
446 sounds physical.

447 Acknowledgements

448 LCPP (Laboratoire Commun de la Prefecture de Police) and LRGP (Laboratoire Réac-
449 tions et Génie des Procédés) are fully acknowledged for TGA measurements and DSC
450 measurements respectively.

451 References

- 452 [1] R. Sikkema, D. Styles, R. Jonsson, B. Tobin, and K.A. Byrne. “A market inventory
453 of construction wood for residential building in Europe – in the light of the Green
454 Deal and new circular economy ambitions”. In: *Sustainable Cities and Society* 90

- 455 (2023), p. 104370. ISSN: 2210-6707. DOI: [https://doi.org/10.1016/j.scs.2022.](https://doi.org/10.1016/j.scs.2022.104370)
456 [104370](https://doi.org/10.1016/j.scs.2022.104370).
- 457 [2] Jakob Hildebrandt, Nina Hagemann, and Daniela Thrän. “The contribution of
458 wood-based construction materials for leveraging a low carbon building sector in
459 europe”. In: *Sustainable Cities and Society* 34 (2017), pp. 405–418. ISSN: 2210-6707.
460 DOI: <https://doi.org/10.1016/j.scs.2017.06.013>.
- 461 [3] Lei Wang, Anne Toppinen, and Heikki Juslin. “Use of wood in green building: a
462 study of expert perspectives from the UK”. In: *Journal of Cleaner Production* 65
463 (2014), pp. 350–361. ISSN: 0959-6526. DOI: [https://doi.org/10.1016/j.jclepro.](https://doi.org/10.1016/j.jclepro.2013.08.023)
464 [2013.08.023](https://doi.org/10.1016/j.jclepro.2013.08.023).
- 465 [4] C. A. Koufopoulos, A. Lucchesi, and G. Maschio. “Kinetic modelling of the pyrolysis
466 of biomass and biomass components”. en. In: *Can. J. Chem. Eng.* 67.1 (Feb. 1989),
467 pp. 75–84. ISSN: 00084034, 1939019X. DOI: [10.1002/cjce.5450670111](https://doi.org/10.1002/cjce.5450670111).
- 468 [5] Carmen Branca and Colomba Di Blasi. “Kinetics of the isothermal degradation of
469 wood in the temperature range 528–708 K”. en. In: *J. Anal. Appl. Pyrolysis* (2003),
470 p. 13.
- 471 [6] Zhihua Chen, Mian Hu, Xiaolei Zhu, Dabin Guo, Shiming Liu, Zhiquan Hu, Bo
472 Xiao, Jingbo Wang, and Mahmood Laghari. “Characteristics and kinetic study on
473 pyrolysis of five lignocellulosic biomass via thermogravimetric analysis”. In: *Biore-*
474 *source Technology* 192 (2015), pp. 441–450. ISSN: 0960-8524. DOI: [https://doi.](https://doi.org/10.1016/j.biortech.2015.05.062)
475 [org/10.1016/j.biortech.2015.05.062](https://doi.org/10.1016/j.biortech.2015.05.062).
- 476 [7] B. M. Wagenaar, Wolter Prins, and W.P.M. van Swaaij. “Pyrolysis of biomass in
477 the rotating cone reactor: modelling and experimental justification”. In: *Chemical*
478 *Engineering Science* 49 (1994), pp. 5109–5126.
- 479 [8] Lucas Terrei, Guillaume Gerandi, Hassan Flity, Virginie Tihay-Felicelli, Zoubir
480 Acem, Gilles Parent, and Paul-Antoine Santoni. “Experimental and numerical multi-
481 scale study of spruce wood degradation under inert atmosphere”. en. In: *Fire Safety*
482 *Journal* 130 (June 2022), p. 103598. ISSN: 03797112. DOI: [10.1016/j.firesaf.](https://doi.org/10.1016/j.firesaf.2022.103598)
483 [2022.103598](https://doi.org/10.1016/j.firesaf.2022.103598).
- 484 [9] H. Thunman, B. Leckner, F. Niklasson, and F. Johnsson. “Combustion of wood
485 particles - a particle model for eulerian calculations”. en. In: *Combustion and Flame*
486 129.1-2 (Apr. 2002), pp. 30–46. ISSN: 00102180. DOI: [10.1016/S0010-2180\(01\)](https://doi.org/10.1016/S0010-2180(01)00371-6)
487 [00371-6](https://doi.org/10.1016/S0010-2180(01)00371-6).
- 488 [10] S. Benkorichi, T. Fateh, F. Richard, J.-L. Consalvi, and A. Nadjai. “Investigation
489 of thermal degradation of pine needles using multi-step reaction mechanisms”. en.
490 In: *Fire Safety Journal* 91 (July 2017), pp. 811–819. ISSN: 03797112. DOI: [10.1016/](https://doi.org/10.1016/j.firesaf.2017.03.058)
491 [j.firesaf.2017.03.058](https://doi.org/10.1016/j.firesaf.2017.03.058).
- 492 [11] Carmen Branca, Alessandro Albano, and Colomba Di Blasi. “Critical evaluation
493 of global mechanisms of wood devolatilization”. en. In: *Thermochimica Acta* 429.2
494 (May 2005), pp. 133–141. ISSN: 00406031. DOI: [10.1016/j.tca.2005.02.030](https://doi.org/10.1016/j.tca.2005.02.030).
- 495 [12] Morten Gunnar GrÅ_nli, GÅ_jbor VÅ_rhegyi, and Colomba Di Blasi. “Thermogravi-
496 metric Analysis and Devolatilization Kinetics of Wood”. In: *Ind. Eng. Chem. Res.*
497 41.17 (Aug. 2002). Publisher: American Chemical Society, pp. 4201–4208. ISSN:
498 0888-5885. DOI: [10.1021/ie0201157](https://doi.org/10.1021/ie0201157).

- 499 [13] T. Kashiwagi, T.J. Ohlemiller, and K. Werner. “Effects of external radiant flux and
500 ambient oxygen concentration on nonflaming gasification rates and evolved products
501 of white pine”. en. In: *Combustion and Flame* 69.3 (Sept. 1987), pp. 331–345. ISSN:
502 00102180. DOI: [10.1016/0010-2180\(87\)90125-8](https://doi.org/10.1016/0010-2180(87)90125-8).
- 503 [14] Chris Lautenberger and Carlos Fernandez-Pello. “Generalized pyrolysis model for
504 combustible solids”. In: *Fire Safety Journal* 44.6 (2009), pp. 819–839. ISSN: 0379-
505 7112. DOI: <https://doi.org/10.1016/j.firesaf.2009.03.011>.
- 506 [15] Stanislav I. Stoliarov, Sean Crowley, Richard N. Walters, and Richard E. Lyon.
507 “Prediction of the burning rates of charring polymers”. In: *Combustion and Flame*
508 157.11 (2010), pp. 2024–2034. ISSN: 0010-2180. DOI: [https://doi.org/10.1016/
509 j.combustflame.2010.03.011](https://doi.org/10.1016/j.combustflame.2010.03.011).
- 510 [16] Lucas Bustamante Valencia. “Experimental and numerical investigation of the ther-
511 mal decomposition of materials at three scales: application to polyether polyurethane
512 foam used in upholstered furniture”. PhD thesis. ISAE-ENSMA Ecole Nationale
513 Supérieure de Mécanique et d’Aérotechnique-Poitiers, 2009.
- 514 [17] Franz Richter and Guillermo Rein. “A multiscale model of wood pyrolysis in fire
515 to study the roles of chemistry and heat transfer at the mesoscale”. In: *Combustion
516 and Flame* 216 (2020), pp. 316–325. ISSN: 0010-2180. DOI: [https://doi.org/10.
517 1016/j.combustflame.2020.02.029](https://doi.org/10.1016/j.combustflame.2020.02.029).
- 518 [18] Chris Lautenberger and Carlos Fernandez-Pello. “A model for the oxidative py-
519 rolysis of wood”. In: *Combustion and Flame* 156.8 (2009), pp. 1503–1513. ISSN:
520 0010-2180. DOI: <https://doi.org/10.1016/j.combustflame.2009.04.001>.
- 521 [19] Haiping Yang, Rong Yan, Hanping Chen, Dong Ho Lee, and Chuguang Zheng.
522 “Characteristics of hemicellulose, cellulose and lignin pyrolysis”. en. In: *Fuel* 86.12-13
523 (Aug. 2007), pp. 1781–1788. ISSN: 00162361. DOI: [10.1016/j.fuel.2006.12.013](https://doi.org/10.1016/j.fuel.2006.12.013).
- 524 [20] Vaibhav Dhyani and Thallada Bhaskar. “A comprehensive review on the pyrolysis
525 of lignocellulosic biomass”. en. In: *Renewable Energy* 129 (Dec. 2018), pp. 695–716.
526 ISSN: 09601481. DOI: [10.1016/j.renene.2017.04.035](https://doi.org/10.1016/j.renene.2017.04.035).
- 527 [21] Donald W. Marquardt. “An Algorithm for Least-Squares Estimation of Nonlinear
528 Parameters”. en. In: *Journal of the Society for Industrial and Applied Mathematics*
529 11.2 (June 1963), pp. 431–441. ISSN: 0368-4245, 2168-3484. DOI: [10.1137/0111030](https://doi.org/10.1137/0111030).
- 530 [22] Junhui Gong and Lizhong Yang. “A Review on Flaming Ignition of Solid Com-
531 bustibles: Pyrolysis Kinetics, Experimental Methods and Modelling”. In: *Fire Tech-
532 nology* (2022), pp. 1–98.
- 533 [23] J. Rath, M.G. Wolfinger, G. Steiner, G. Krammer, F. Barontini, and V. Cozzani.
534 “Heat of wood pyrolysis”. In: *Fuel* 82.1 (2003), pp. 81–91. ISSN: 0016-2361. DOI:
535 [https://doi.org/10.1016/S0016-2361\(02\)00138-2](https://doi.org/10.1016/S0016-2361(02)00138-2).
- 536 [24] Lucas Terrei, Zoubir Acem, Véronique Marchetti, Paul Lardet, Pascal Boulet, and
537 Gilles Parent. “In-depth wood temperature measurement using embedded thin wire
538 thermocouples in cone calorimeter tests”. en. In: *International Journal of Thermal
539 Sciences* 162 (Apr. 2021), p. 106686. ISSN: 12900729. DOI: [10.1016/j.ijthermalsci.
540 2020.106686](https://doi.org/10.1016/j.ijthermalsci.2020.106686).

541 [25] Yves Jannot and Alain Degiovanni. “An improved model for the parallel hot wire:
542 Application to thermal conductivity measurement of low density insulating mate-
543 rials at high temperature”. en. In: *International Journal of Thermal Sciences* 142
544 (Aug. 2019), pp. 379–391. ISSN: 12900729. DOI: [10.1016/j.ijthermalsci.2019.](https://doi.org/10.1016/j.ijthermalsci.2019.04.026)
545 [04.026](https://doi.org/10.1016/j.ijthermalsci.2019.04.026).

546 [26] Zoubir Acem, Damien Brissinger, Anthony Collin, Gilles Parent, Pascal Boulet,
547 Thi Hay Yen Quach, Benjamin Batiot, Franck Richard, and Thomas Rogaume.
548 “Surface temperature of carbon composite samples during thermal degradation”.
549 In: *International Journal of Thermal Sciences* 112 (2017), pp. 427–438. ISSN: 1290-
550 0729. DOI: <https://doi.org/10.1016/j.ijthermalsci.2016.11.007>.

551 [27] Hassan Flity, Yves Jannot, Lucas Terrei, Paul Lardet, Vincent Schick, Zoubir Acem,
552 and Gilles Parent. “Thermal conductivity parallel and perpendicular to fibers di-
553 rection and heat capacity measurements of eight wood species up to 160 °C”. In:
554 *International Journal of Thermal Sciences* submitted (2023).

555 [28] Yves Jannot, Alain Degiovanni, Vincent Schick, and Johann Meulemans. “Apparent
556 thermal conductivity measurement of anisotropic insulating materials at high tem-
557 perature by the parallel hot-wire method”. en. In: *International Journal of Thermal*
558 *Sciences* (2021), p. 9.

559 [29] S. Lagüela, P. Bison, F. Peron, and P. Romagnoni. “Thermal conductivity mea-
560 surements on wood materials with transient plane source technique”. en. In: *Ther-*
561 *mochimica Acta* 600 (Jan. 2015), pp. 45–51. ISSN: 00406031. DOI: [10.1016/j.tca.](https://doi.org/10.1016/j.tca.2014.11.021)
562 [2014.11.021](https://doi.org/10.1016/j.tca.2014.11.021).

563 [30] V. Hankalin, T. Ahonen, and R. Raiko. “On thermal properties of a pyrolysing
564 wood particle”. English. In: *Finnish-Swedish Flame Days 2009, January 28-29, 2009,*
565 *Naantali, Finland*. 2009, 16 p.

566 [31] S. Korkut, A. Aytin, Ç. Tasdemir, and L. Gurau. *The transverse thermal conductivity*
567 *coefficients of wild cherry wood heat-treated using the thermowood method*. Pro Ligno,
568 Brasov, Romania, pp. 679-683. Nov. 2015.

569 [32] Hamiyet Kol. “The Transverse Thermal Conductivity Coefficients of Some Hard-
570 wood Species Grown in Turkey”. en. In: *Forest Products Journal* 59.10 (Oct. 2009),
571 pp. 58–63. ISSN: 0015-7473. DOI: [10.13073/0015-7473-59.10.58](https://doi.org/10.13073/0015-7473-59.10.58).

572 [33] Anna Dupleix, Andrzej Kusiak, Mark Hughes, and Frédéric Rossi. “Measuring the
573 thermal properties of green wood by the transient plane source (TPS) technique”.
574 en. In: *Holzforschung* 67.4 (May 2013), pp. 437–445. ISSN: 1437-434X, 0018-3830.
575 DOI: [10.1515/hf-2012-0125](https://doi.org/10.1515/hf-2012-0125).

576 **Figure captions**

577 **Fig.1:** Mean normalized mass loss and mean normalized mass loss rate as a
578 function of temperature for the different heating rates: 5, 10 and 20
579 °C · min⁻¹. 3

580 **Fig.2:** Comparison between the numerical and experimental results for dif-
581 ferent heating rates. A₁, A₂, and A₃ are the pseudo-components of
582 wood, while C₂ and C₃ are two char constituents. 6

583	Fig.3:	Comparison between the normalized heat flux measured by DSC and the numerical heat flux predicted with the model using (a) 3 reactions and (b) 4 reactions. The experimental data is the average of three repeatability tests.	8
584			
585			
586			
587	Fig.4:	Boundary conditions of a sample exposed to the cone calorimeter. . .	9
588	Fig.5:	Comparison between numerical and experimental in-depth temperature within the calcium silicate sample at two different heat fluxes. .	12
589			
590	Fig.6:	Comparison between the estimated and the measured thermal conductivity of the calcium silicate [25].	13
591			
592	Fig.7:	Comparison between numerical and experimental mass loss and ML-RPUA for wood tests at different heat fluxes.	13
593			
594	Fig.8:	Comparison between numerical and experimental in-depth temperature within the wood samples at different heat fluxes.	14
595			